Journal of Geophysical Research: Space Physics

RESEARCH ARTICLE
10.1029/2017JA025147

Tailward Propagation of Magnetic Energy Density Variations With Respect to Substorm Onset Times

John C. Coxon[1], Mervyn P. Freeman[2], Caitriona M. Jackman[1], Colin Forsyth[3], I. Jonathan Rae[3], and Robert C. Fear[1]

[1]Department of Physics and Astronomy, University of Southampton, Southampton, UK, [2]British Antarctic Survey, Cambridge, UK, [3]UCL Mullard Space Science Laboratory, Dorking, UK

Key Points:
- Lobe magnetic energy density increases prior to substorms and decreases following onset
- The change in magnetic energy density is first seen within 9 R_E and then propagates downtail
- On average, the decrease in near-tail energy density is observed before the ground onset

Correspondence to:
J. C. Coxon,
work@johncoxon.co.uk

Citation:
Coxon, J. C., Freeman, M. P., Jackman, C. M., Forsyth, C., Rae, I. J., & Fear, R. C. (2018). Tailward propagation of magnetic energy density variations with respect to substorm onset times. *Journal of Geophysical Research: Space Physics*, *123*, 4741–4754. https://doi.org/10.1029/2017JA025147

Received 20 DEC 2017
Accepted 15 MAY 2018
Accepted article online 21 MAY 2018
Published online 15 JUN 2018
Corrected 29 JUN 2018

This article was corrected on 29 JUN 2018. See the end of the full text for details.

Abstract During geomagnetic substorms, around 10^{15} J of energy is extracted from the solar wind and processed by the Earth's magnetosphere. Prior to the onset of substorm expansion phases, this energy is thought to be largely stored as an increase in the magnetic field in the magnetotail lobes. However, how, when, and where this energy is stored and released within the magnetotail is unclear. Using data from the Cluster spacecraft and substorm onsets from Substorm Onsets and Phases from Indices of the Electrojet (SOPHIE), we examine the variation in the lobe magnetic energy density with respect to substorm onset for 541 isolated onsets. Based on a cross-correlation analysis and a simple model, we deduce the following: On average, the magnetic energy density increases approximately linearly in the hour preceding onset and decreases at a similar rate after onset. The timing and magnitude of these changes varies with downtail distance, with observations from the mid-tail ($X \lessapprox -9\ R_E$) showing larger changes in the magnetic energy density that occur $\sim$ 20 min after changes in the near-tail ($X \gtrapprox -9\ R_E$). The decrease in energy density in the near-tail region is observed before the ground onset identified by SOPHIE, implying that the substorm is driven from the magnetotail and propagates into the ionosphere. The implication of these results is that energy in the near-tail region is released first during the substorm expansion phase, with energy conversion propagating away from the Earth with time.

1. Introduction

Substorms are global reconfigurations of Earth's magnetosphere that transfer $\sim 10^{15}$ J of energy stored in the magnetotail into energizations of plasma, atmospheric heating, and brilliant auroral displays. Two phases of a substorm were first outlined by Akasofu (1964): the existence of the expansion phase, which is defined by auroral expansion in the night sky, and the recovery phase, which comes after the expansion phase and is the return of the aurora to their quiescent state. Later, McPherron (1970) used magnetograms to demonstrate the existence of a third phase of the substorm called the growth phase, during which energy is accumulated within the magnetotail prior to the expansion phase. In this paper, the term *substorm onset* will be used to refer to substorm expansion phase onset.

It has previously been shown that magnetic flux is added to the magnetosphere during the growth phase of a substorm, and then this flux is removed from the magnetosphere again during the substorm expansion phase (e.g., Baker et al., 1996; Hones, 1979, and references therein) in what is now known as the substorm cycle. This can be interpreted (Freeman & Southwood, 1988; Lockwood & Cowley, 1992; Siscoe & Huang, 1985) as a time-dependent revision of the Dungey cycle (Dungey, 1961) with unbalanced dayside and nightside reconnection rates in which magnetic flux (and thus energy) is stored in the magnetosphere when the dayside reconnection rate exceeds the nightside rate during the growth phase and is then released again when the nightside reconnection exceeds the dayside rate in the expansion/recovery phase. This theory has been confirmed experimentally in terms of magnetic flux, as authors have observed the polar cap area (and proxies thereof) varying with dayside reconnection rate and substorm onsets (e.g., Clausen et al., 2012; Coxon et al., 2014a; DeJong et al., 2007; Hubert et al., 2006; Milan et al., 2007).

It has long been thought that the lobes are the location of the energy that is stored in the magnetosphere prior to being dissipated by a substorm (e.g., Baker et al., 1997; McPherron et al., 1973), but there is some debate about this. The temperature and pressure of the plasma sheet increases during the growth phase (Forsyth et al., 2014), indicating that the energy added to the magnetosphere during the growth phase is

contained within the lobes and within the plasma sheet. Baker et al. (1997) calculated that the amount of energy in the plasma sheet was not large enough to provide the entire substorm's energy budget, being approximately 5 times too small, as opposed to the lobes, which contained approximately 10 times more energy than needed. Snekvik et al. (2012) reported that sometimes the magnetic pressure in the lobe did not change in the substorm growth phase, which they identified through magnetotail current sheet thinning. In addition, Akasofu (2013, 2017) made theoretical arguments that the substorm energy is stored in the inner magnetosphere rather than in the magnetotail lobes by estimating the energy content of the magnetotail assuming a magnetic field of 30 nT and a certain magnetotail volume. Miyashita et al. (2015) argued that Akasofu (2013) should instead have considered the energy added to the magnetotail prior to substorm onset (which is the approach we adopt in this paper) and wrote that this, alongside a failure to properly account for the length of the expansion phase and the net Poynting flux, rendered Akasofu (2013) fundamentally flawed.

The factors controlling the intensity of a substorm (by which we mean the magnitude of the magnetic bay measured in the *AL* index or more recent analogues such as the *SML* index (Newell & Gjerloev, 2011) have been the subject of much debate in the literature. Some authors have argued that the amount of energy stored in the growth phase is always approximately the same value: Kallio et al. (2000) concluded that $\sim 5 \times 10^{14}$ J was stored in the growth phase regardless of the intensity of the substorm and argued that any difference in intensity must therefore come from the magnitude of southward interplanetary magnetic field (IMF) during the expansion phase. Kallio et al. (2000) further argued that this was substantiated by previous results showing that the integration of IMF B_Z in the solar wind determined the time-integrated *AL* index (Holzer & Slavin, 1979), but it is important to note that the result of Holzer and Slavin (1979) can also be explained by the fact that on long enough timescales, the dayside and nightside reconnection rates are approximately equivalent (e.g., Cowley & Lockwood, 1992; Coxon, Milan, et al., 2016) and the *AL* index can be considered a proxy of nightside reconnection rate (e.g., Coxon et al., 2014b; Holzer et al., 1986). We argue that this latter interpretation is more likely, as the former argument seems to rely on instantaneous transmission of information between the magnetopause and the magnetotail, whereas previous studies suggest that a more reasonable timescale for this is $\sim$ 1 hr (e.g., Browett et al., 2017; Cowley & Lockwood, 1992). Additionally, previous authors have found that the intensity of a substorm is larger when the amount of open magnetic flux in the polar cap is larger at onset (Coxon et al., 2014a; Milan et al., 2009), as well as that the intensity of a substorm is weakly correlated to the plasma sheet temperature at onset (Forsyth et al., 2014). These results imply that substorms are more intense when more energy is stored within the magnetosphere at the point of onset, which seems to contradict the result of Kallio et al. (2000).

A substorm dissipates energy through several mechanisms: increasing the energy of the ring current, Joule heating of the ionosphere, particle precipitation causing aurora, in plasmoids ejected downtail, and heating of the plasma sheet (e.g., Akasofu, 1981; Østgaard et al., 2002). The way in which the energy is partitioned between these mechanisms has been the focus of much research, with estimates of the relative importance of each varying hugely. Tanskanen et al. (2002) found that 30% of the energy input to the magnetosphere by the solar wind ended up Joule heating the ionosphere. Østgaard et al. (2002) measured the contributions of ionospheric Joule heating E_J, auroral precipitation E_A, and ring current energization E_R and found the sum of those three E_{O02}, finding that the relative contributions of the three were $E_J = 56\%$, $E_A = 29\%$, and $E_R = 15\%$. The average energy dissipated by a substorm by these three mechanisms was found to be $E_{O02} = 7.7 \times 10^{15}$ J, which was higher than the 5×10^{14} J estimated by Baker et al. (1997). Weiss et al. (1992) also estimated the amount of plasma sheet heating $E_{PS} \approx 0.25E_J$ and the amount of energy released in plasmoids downtail $E_P \approx 0.1E_J$ but, in contrast to Østgaard et al. (2002), found that ring current energization $E_R = 0.5E_J$ and $E_A = 0.2E_J$, such that ring current energization was the second largest energy sink. Forsyth et al. (2016) found that only 50% of substorms result in an increase in the electron content of the radiation belts, which might suggest that the percentage contribution of radiation belt energization is variable from event to event. Forsyth et al. (2014) showed that the increase in plasma sheet temperature before onset accounts for 1.5–7% of substorm energy. Axford (1999) estimated that E_P was 90% of the total energy budget of a substorm, but Ieda et al. (1998) estimated $E_P \approx 10^{15}$ J and Weiss et al. (1992), $E_P \approx 10^{14}$ J. Compared to the total substorm energy calculated by Østgaard et al. (2002) and assuming that the plasma sheet heating is negligible, this accounts for $\sim 10\%$ of Østgaard et al.'s (2002) substorm energy (Ieda et al., 1998) or $\sim 1\%$ of Østgaard et al.'s (2002) substorm energy (Weiss et al., 1992), both much smaller estimates. The amount of magnetic flux added during the growth phase can be estimated by parameterizations based on solar wind data (Milan et al., 2012), as can the amount of energy added during this time (Perreault & Akasofu, 1978).

Table 1
A Tabulation of Previous Work on the Partitioning of the Substorm Energy Budget

Author	E_J	E_A	E_R	E_{PS}	E_P	Total energy dissipated
Weiss et al. (1992)	10^{15} J	$0.2E_J$	$0.5\ E_J$	$0.25\ E_J$	$0.1\ E_J$	
Baker et al. (1997)	$10^{10}-10^{11}$ W	$10^{9}-10^{10}$ W	$10^{11}-10^{12}$ W - E_P		$10^{11}-10^{12}$ W - E_R	5×10^{14} J
Ieda et al. (1998)					10^{15} J	
Axford (1999)					90%	
Østgaard et al. (2002)	56%	29%	15%			7.7×10^{15} J
Tanskanen et al. (2002)	30%					

Baker et al. (1997) found that the rate of energy lost to ring current injections and plasmoids was $10^{11}-10^{12}$ W, with ionospheric Joule heating $10^{10}-10^{11}$ W; auroral precipitation $10^{9}-10^{10}$ W; and auroral luminosity and kilometric radiation less than 10^{9} W. A summary of the literature on substorm energy partitioning is presented in Table 1.

The magnetospheric processes associated with substorm onset and their relative timings have been the subject of much controversy in the literature. It is generally accepted that the closure of magnetic flux occurs at a near-Earth neutral line (NENL) at a distance $>20R_E$ downtail (Baker et al., 1996). However, the substorm onset arc is normally located equatorward of the auroral boundary; thus, the first brightening of the aurora is not necessarily associated with the closure of magnetic flux. Numerous studies have suggested that this initial brightening is associated with a plasma instability in the near-tail region at $<10R_E$ (e.g., Lui, 1996; Lui et al., 1992) causing a current disruption (CD; the CD model). The Time History of Events and Macroscale Interactions during Substorms (THEMIS) spacecraft were launched to attempt to differentiate between the NENL and CD models. Early evidence supported the NENL model (Angelopoulos et al., 2008), but Lui (2009) subsequently reinterpreted Angelopoulos et al.'s (2008) findings as evidence for the CD model, after which Angelopoulos et al. (2008) argued that Lui's (2009) reinterpretation was flawed. Modeling has shown that when magnetic flux in the dayside magnetopause is eroded, sunward convection occurs to replenish the flux on the dayside but depletes the flux in the magnetotail, which leads to strong current sheet thinning and an increase in the crosstail current, suggesting that the instability leading to substorm onset is in the near-Earth tail (Hsieh & Otto, 2014, 2015), and this is substantiated by recent observations (Sun et al., 2017). Hsieh and Otto (2014) noted that the difference between field lines from $10R_E$ and $20R_E$, when mapped to the ionosphere, was small enough that they could not differentiate between the two competing paradigms. Recent studies show that almost all substorm onset arcs show the signatures of a near-tail plasma instability (Kalmoni et al., 2017; Nishimura et al., 2016), but whether this instability is triggered as a result of incoming plasma flows from a small-scale reconnection site, or whether it is simply due to changing plasma conditions, remains an open question.

In this paper, we utilize Cluster observations of Earth's magnetic field made within the magnetotail lobes on either side of substorm onsets determined by Substorm Onsets and Phases from Indices of the Electrojet (SOPHIE; section 2). We conduct superposed epoch analyses of the magnetic energy density either side of 541 substorm expansion phase onsets (section 3), before subdividing the data by distance downtail (section 4). We interpret the results using a simple model (section 5) and discuss the ramifications of our results in the context of previous studies (section 6) before concluding (section 7).

2. Data

The Cluster constellation was launched into orbit by two Soyuz rockets in 2000, with data available from the start of 2001 (Escoubet et al., 2001). The constellation, comprising four satellites, was originally launched into an orbit with a perigee of $4R_E$ and an apogee of $19.6R_E$ in 2001 (Escoubet et al., 2001). This orbit has evolved as the mission has progressed, with the apogee becoming larger and moving down from the plane of the ecliptic such that the spacecraft has spent much more time in the southern lobe of the magnetotail than in the northern lobe. We identify the lobe using Cluster data using a technique that identifies the lobe based purely on thresholds in magnetometer data (Coxon, Jackman, et al., 2016). The technique outlined in Coxon, Jackman, et al. (2016) works by identifying periods where the magnetic field is relatively strong and relatively invariant when the spacecraft is at least $8\ R_E$ downtail on Earth's nightside. In this paper, we employ magnetic

field data taken when the Cluster 1 (C1) spacecraft was in the lobe between 2001 and 2013 inclusive. We use magnetic field data because we are investigating the amount of energy stored in the lobes by the addition of magnetic flux, and we only use C1 in order to avoid considering substorms more than once.

We identify substorm phases using the SOPHIE method (Forsyth et al., 2015). The SOPHIE method works by taking the SuperMAG-derived geomagnetic indices *SMU* and *SML* (equivalents to *AU* and *AL*) and using the time derivative of the *SML* index to create a list of the growth, expansion, and recovery phases of substorms from 1996 to 2014. In this paper, SOPHIE data coincident with the Cluster data are utilized to identify isolated substorm expansion phases (i.e., those expansion phases preceded by a growth phase instead of preceded by a recovery phase). We adopt the criterion that C1 has to remain in the lobe for 3 hr either side of a substorm onset for that onset to be considered in our analysis. We choose this length of time such that we can effectively detrend the magnetic field measurements to remove any effect of the spacecraft motion: As C1 moves toward Earth, the magnetic field strength increases, and as it moves away, the magnetic field strength decreases. This is not a signature of substorm activity, and therefore, we outline a method for removing this effect in section 3.

We also employ data from the OMNI data set, namely, the IMF vector and the solar wind flow speed, in order to calculate the dayside reconnection rate ϕ_D given by the equation of Milan et al. (2012). We modify the term for ϕ_D given therein such that

$$\Phi_D = L_{\text{eff}}(V_X) V_X B_{YZ} \left| \sin^{\frac{9}{2}}\left(\frac{\theta}{2}\right) \right|, \tag{1}$$

where V_X is the solar wind speed, B_{YZ} is the transverse component of the IMF, θ is the clock angle (the angle between the IMF vector projected into the GSM (geocentric solar magnetospheric) *Y*-*Z* plane and the *Z* axis), R_E is the radius of Earth, and $L_{\text{eff}}(V_X)$ is an effective length scale

$$L_{\text{eff}}(V_X) = 3.8 R_E \left(\frac{V_X}{4 \times 10^5 \text{m/s}} \right)^{\frac{1}{3}}. \tag{2}$$

3. Superposed Epoch Analysis of the Magnetic Energy Density in the Lobe

Between 2001 and 2013 we use SOPHIE to identify 541 substorm onsets that occurred while C1 was in the magnetotail lobes. Figure 1a shows a superposed epoch analysis of the magnetic energy density U_B through a 6-hr window centered on substorm onset: The solid blue line is the mean of U_B, and the shaded area is the standard error on the mean. The energy density can be seen to decrease through the first 90 min of the epoch and then to increase through the rest of the epoch.

We investigate the shape of Figure 1a in more detail by constructing a simple dipole model (Walker & Russell, 1995) such that

$$B_X = 3xzM_z R^{-5}, \tag{3}$$

$$B_Y = 3yzM_z R^{-5}, \tag{4}$$

$$B_Z = (3z^2 - R^2) M_z R^{-5}, \tag{5}$$

where x, y, and z are the coordinates of C1; M_z is the dipole magnetic moment of Earth; and R is the radial distance of C1 from Earth. We evaluate this vector for each of the data contributing to Figure 1a and then perform the same analysis of these synthesized magnetic data as the analysis performed on the real magnetic data, thus producing Figure 1c. Figure 1c shows that the magnetic energy density U_D of this simple dipole model follows the same general trend as Figure 1a, which indicates that this trend is due to the motion of C1 through the magnetotail, rather than substorm-related effects.

In order to isolate the substorm-related perturbation, we assume that it is negligible beyond 1 hr of onset and subtract a second-order polynomial fit to the data excluding the 1 hr before and after the onset (the solid orange line in Figure 1a) from the observations. The difference between the U_B and our fit, which we denote ΔU_B, is shown in Figure 1b and thus shows only the change in energy density due to the substorm. The blue and red lines in Figure 1a diverge by more than the standard error on the mean, giving confidence that the increase and decrease on either side of substorm onset is due to a physical phenomenon.

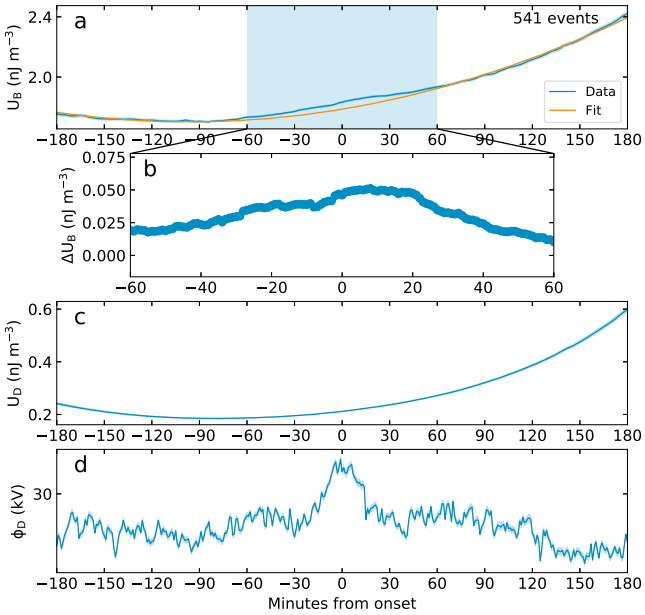

Figure 1. Superposed epoch analysis of the magnetic energy density, dipole energy density, and dayside reconnection rate from 541 substorms. (a) The magnetic energy density in the magnetotail lobes U_B (blue). The orange line is a fit to the blue line (ignoring data within an hour of substorm onset). (b) The difference between the blue and orange lines from panel a, denoted ΔU_B. (c) The magnetic energy density of the calculated dipole field U_D. (d) The reconnection rate ϕ_D, calculated from Milan et al. (2012) with the correction described in section 2. Panels a, c, and d show 3 hr either side of substorm onset, whereas panel b shows 1 hr either side of substorm onset. The standard error on the mean is plotted as a shaded blue area on either side of the blue line in panels a, c, and d.

In Figure 1b, ΔU_B starts at $\sim$ 0.02 nJ/m^3, and in fact Figure 1a shows that the superposed epoch analysis and fit lines diverge after $T = -75$ min. This could indicate that our fit line from Figure 1a has not completely removed the background energy density, or alternatively, it might indicate that although a substantial amount of energy ($\sim$ 0.03 nJ/m^3) is added in the hour prior to expansion phase onset, some energy has been added prior to that stage. ΔU_B increases up to substorm onset, then plateaus between $T = 0$ min and $T = 20$ min before decreasing back to pre-onset values. Once ΔU_B begins to decrease, it takes 40 min to decrease to under the value at the start of the interval, and inspection of Figure 1a shows that the fit line and the observed line converge at $T \approx 75$ min.

Figure 1d shows the superposed epoch analysis of dayside reconnection rate ϕ_D as inferred from our modified version of Milan et al. (2012; see section 2). ϕ_D stays fairly steady at the start of the epoch, starting to increase at $T \approx -30$ min until $T \approx -5$ min. ϕ_D plateaus during $-5 < T < 5$ min and then decreases until around $T \approx 15$ min, at which point it levels out at the pre-onset value. Previous superposed epoch analyses of dayside reconnection rate also show it decreasing after onset (e.g., Coxon et al., 2014a), which might be simply due to the tendency for the IMF to turn northward on average after substorm onset. For a statistical explanation of why this occurs, and why this does not necessarily have implications for the physics of substorm onset, the reader is directed to the paper on the topic by Freeman and Morley (2009).

In summary, we detrend the magnetic field measurements to remove any effect of the spacecraft motion, obtaining the change in energy density due to the substorm ΔU_B. Although the ΔU_B rises toward substorm onset and then falls after substorm onset, consistent with the idea of energy being loaded into the magnetotail and then unloaded again when a substorm begins, there is a $\sim$ 20-min-long plateau immediately after substorm onset. This plateau is not colocated with a similar signature in Φ_D, and we will discuss this feature of the data in more detail in later sections.

4. Superposed Epoch Analyses at Different Downtail Distances

In order to further investigate the timing of the plateau just after substorm onset in Figure 1a, we investigate the effect of downtail distance on the data. To do this, we subdivide the events in our database by the downtail distance of C1 at the point of substorm onset. In order to remove variability due to the position in Y and focus

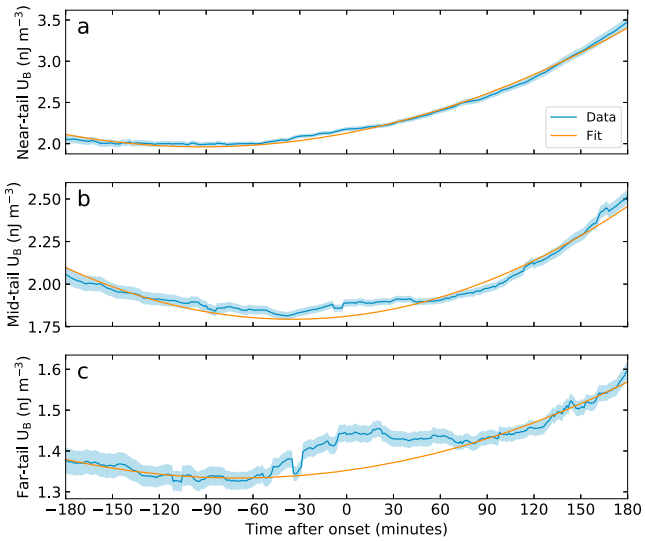

Figure 2. Three panels plotted in the same format as Figure 1a, showing (a) the near-tail data, (b) the mid-tail data, and (c) the far-tail data, with exact bins in X given in the text. The positional ranges refer to the location of C1 at the time of substorm onset, and for all panels, $4 \geq Y \geq -4R_E$.

on effect with downtail distance, we discard events for which C1 was more than 4 R_E away from $Y = 0R_E$, which leaves us with a subset of 195 events. This criterion is intentionally strict, because we are focusing on propagations in the X direction and therefore limiting the range in Y allows us to see these propagations more clearly. If we do not adopt this criterion, the larger range of radial distances introduced by the extent of the data in Y makes it harder to examine propagations in the X direction specifically.

We then further subdivide this subset into three bins of equal size, but of different downtail distance, such that 65 events are contained within each bin. In order to achieve three bins containing 65 events each, the spatial extents are $-6.24 \geq X > -9.20R_E$ (hereafter referred to as near-tail), $-9.20 \geq X > -11.14R_E$ (mid-tail), and $-11.14 \geq X > -17.40R_E$ (far-tail). We choose to subdivide the data by number of events in order to avoid one of our bins being more prone to selection bias (as a result of the law of small numbers fallacy) than the others.

Figure 2a shows the superposed epoch analysis of U_B for the near-tail subset and the fit to that curve, with the standard error on the mean shaded, in the same format as Figure 1a. Figures 2b and 2c are in the same format as 2a but for the mid-tail and far-tail subsets, respectively. In each panel the observed U_B deviates from the fit line by more than the standard error, so we can be confident that the signal we observe is physical.

Figure 3a shows the difference in the two lines for each panel of Figure 2. Blue dots are for the near-tail (Figure 2a), orange dots for the mid-tail (2b), and green dots for the far-tail (2c). The initial and final differences in the energy density for each are given in Table 2, alongside the peak energy density and the time over which the energy density plateaued at that peak.

Next, we performed a cross-correlation analysis. We shifted the mid-tail and far-tail data up to 1 hr in both directions and then compared each lag to the near-tail data. Shifting the mid-tail data by −19 min and shifting the far-tail data by −21 min maximized the correlation coefficients, which indicates that the plateau in the energy density comes later as the observer's downtail distance increases and thus implies that the energy signature is first seen at near-Earth distances and then propagates down the magnetotail. The correlation coefficient for the mid-tail was 0.90 and for the far-tail was 0.54, with p values beneath 10^{-9} in both cases. Figure 3b reproduces the data of Figure 3a but with the time lags found from the cross-correlation analysis applied to the mid-tail and far-tail data and then all three data sets translated by 15 min such that the plateaus center on the time of substorm onset identified by the SOPHIE method. We also translate ΔU_B by −0.025 nJ/m^3 for the mid-tail and by −0.04 nJ/m^3 for the far-tail data to give the best agreement by eye with the near-tail data (which are not translated in ΔU_B). This indicates that the signature in the energy density due to the substorm gets larger as it propagates down the magnetotail. Overlaying the three data sets in this manner gives a good agreement for the decrease in the energy density after onset.

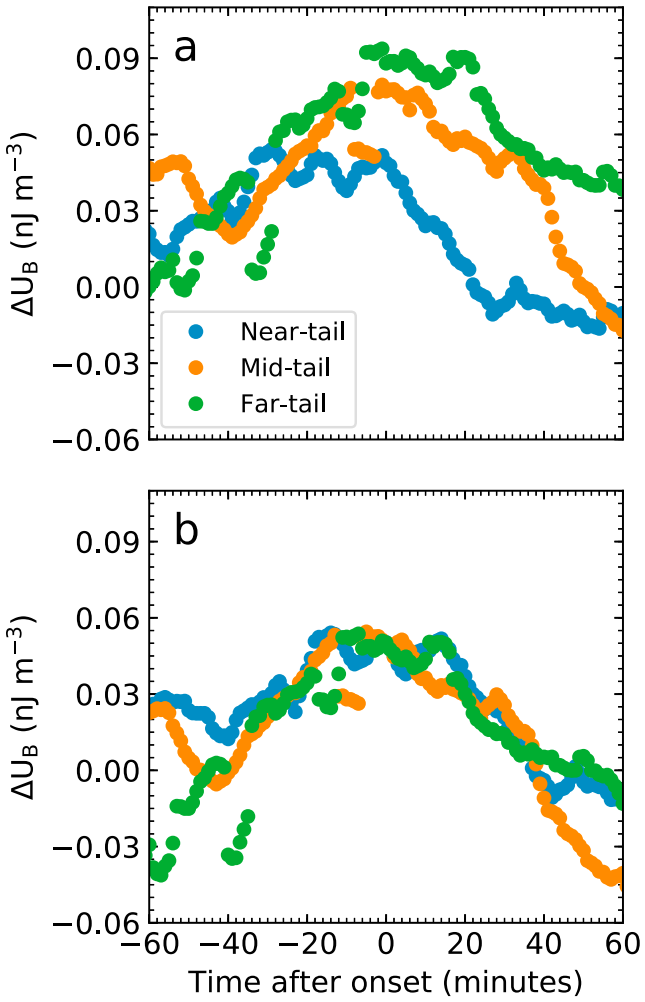

Figure 3. (a) The polynomial we fit in Figure 2 (orange line) subtracted from the superposed data (blue line) for each panel of Figure 2, color coded and overlaid. (b) The data from Figure 3a, translated in T by 15 min and ΔU_B by 0 nJ/m^3 (near-tail), −4 min and −0.025 nJ/m^3 (mid-tail), and −6 min and −0.04 nJ/m^3 (far-tail).

5. A Simple Model of Observed Magnetic Energy Density During Substorms

In order to investigate the plateaus in ΔU_B observed in Figures 1b and 3, we now construct a simple model of the behavior of the energy density in the magnetotail lobes during a substorm. The algorithm used to construct this model is shown in Figure 4. In the model, we assume that the change in energy density due to a substorm is a linear increase in energy density in the hour up to onset followed by a linear decrease for the following hour:

$$\Delta U_B = m\left(1 - \frac{|T|}{60}\right) \tag{6}$$

Table 2
Table to Illustrate the Ranges of Energy Density and Lengths of Plateau in Figure 3a

	ΔU_B (nJ/m^3)			Plateau (min)	
Downtail region	Start	Peak	End	Start	End
Near-tail	0.020	0.050	−0.02	−30	0
Mid-tail	0.020[a]	0.075	−0.02	−10	10
Far-tail	0.000	0.090	0.04	−5	20

Note. This energy density occurs at approximately $T = 20$ min.

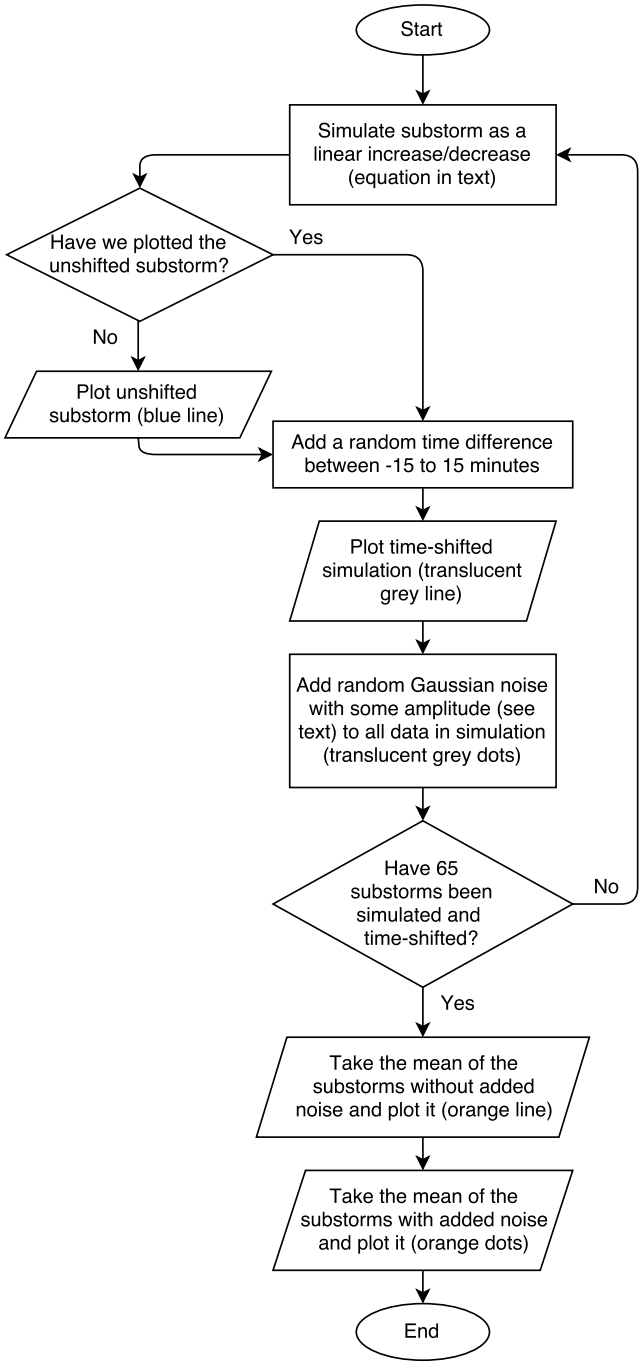

Figure 4. A flowchart describing the construction of the model described in the text. Equation (6) describes the linear increase and decrease, and the plotting described above refers to Figure 5.

where m is the maximum change in energy density in the model; this is plotted for $m = 1$ nJ/m^3 in Figure 5 (red line).

Then, we assume that there is an observational uncertainty in the timing of a substorm with respect to the SOPHIE onset, and we simulate 65 substorm events that are each shifted by a time difference dT randomly sampled from a uniform distribution in the range $-15 \leq dT \leq 15$ min. The 65 simulated measurements with the timing uncertainties are plotted in translucent gray in Figure 5.

We take the mean of the 65 simulations, which is shown as a black line in Figure 5. This black line assumes that the only uncertainty on the measurements is in the timing and that the energy density measurements

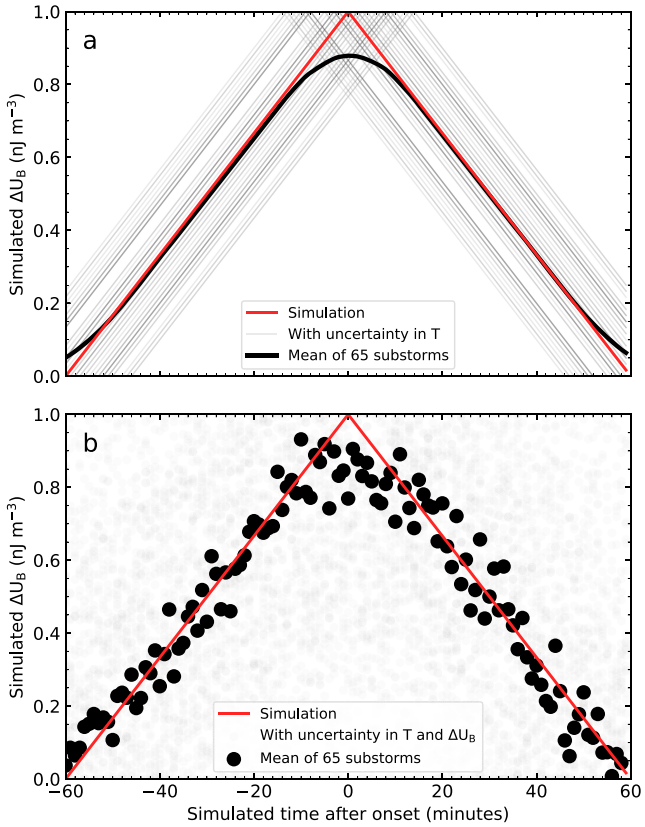

Figure 5. The simple model described in the text, with $m = 1$ nJ/m^3 and $r = 1$. The red line in each panel is the substorm signature with no uncertainty in timing. (a) The 65 simulated substorms with some uncertainty in timing equal to ±15 min (gray lines) and the mean thereof (black line). (b) The 65 simulated substorms with the same error in timing as panel a but with an uncertainty applied to each value of energy density (gray dots) and the mean thereof (black dots).

are perfect. To eliminate this assumption, we add Gaussian noise to each measurement of energy density in each of the 65 substorms and then take the mean, which is shown by the black dots in Figure 5. The noise has zero mean and standard deviation equal to mr, where r is a constant to allow for different amplitudes of noise relative to m.

In Figure 5, $m = 1$ nJ/m^3 and $r = 1$. A plateau is seen centered at $T_{sim} = 0$ min with a width of ~ 20 min, which is a similar width to the plateaus seen in Figures 1b and 3. In Figure 6, we plot our simple model for different values of m and $r = 1$ for each downtail bin. We also add a simple linear term to the model in each plot, in order to closer match the shape of each superposed epoch analysis, as ΔU_B is nonzero at $T = -60$ and 60 min. In Figure 6a, we plot our model with $m = 0.06$ nJ/m^3 and overlay the near-tail data; in Figure 6b, $m = 0.09$ nJ m^{-3} and mid-tail data are overlaid; and in Figure 6c, $m = 0.10$ nJ/m^3 and far-tail data are overlaid. For each of the model outputs, $r = 1$. Much of the variation in each of the panels is captured by the noise level in our simple model, but some variations are not captured—for instance, in each panel, the scatter in the superposed epoch analysis at $T = -40$ min is larger than the scatter in our model.

6. Discussion

Using the set of all 541 events, we find that the energy stored within the magnetotail increases from at least 60 min prior to expansion phase onset, reaching a plateau at $T = 0$ min, and not decreasing until $T = 20$ min. This indicates that the energy density in the magnetotail is increasing and decreasing consistent with the picture of energy being stored and released in the magnetotail lobes, in support of Baker et al. (1985, 1997) and consistent with previous case studies (Caan et al., 1973) and superposed epoch analyses (Caan et al., 1975, 1978) of the magnetic energy density. As magnetic flux is added to the magnetotail, it flares as the lobes expand to accommodate the added flux. This increases the solar wind ram pressure on the magnetotail lobes, which must in turn be balanced by the increase of lobe magnetic pressure, which itself must be balanced by

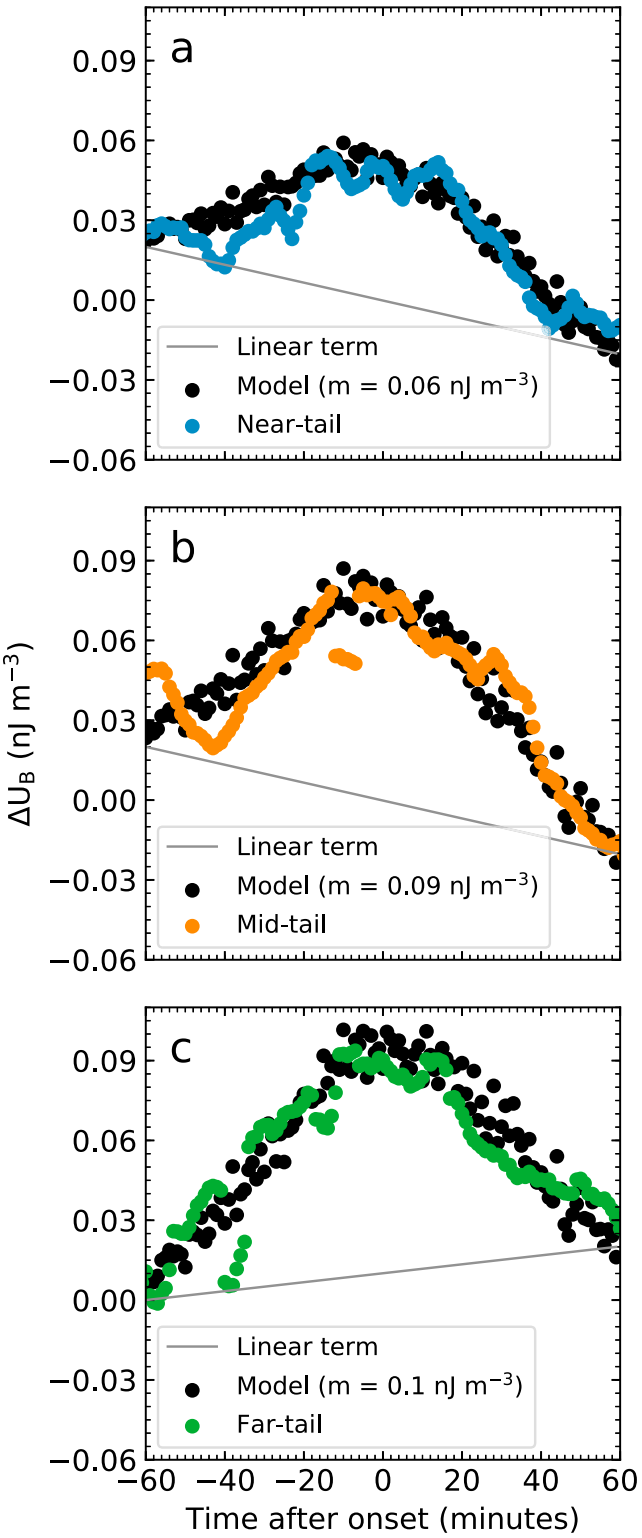

Figure 6. The polynomial we fit in Figure 2 subtracted from the superposed data, plotted for the (a) near-tail, (b) mid-tail, and (c) far-tail subsets. Each panel is shifted by the same time lag as in Figure 3b. In each panel, the simple model described in the text is also plotted, with the *m* parameter set to (a) 0.06 nJ/m^3, (b) 0.09 nJ/m^3, and (c) 0.1 nJ/m^3. For each model, $r = 1$ and a linear term (plotted in gray) is added, as described in the text.

increased plasma sheet pressure (e.g., Forsyth et al., 2014; Sun et al., 2017, and references therein). Previous studies have found that, on average, the plasma sheet pressure increases prior to substorm onset (Forsyth et al., 2014), but a survey of THEMIS data found that in almost 40% of substorms the plasma sheet pressure decreased during the growth phase at downtail distances $7.5 \lesssim R \lesssim 12R_E$ (Sun et al., 2017), although it should be noted that this effect was more pronounced on the dawn and dusk flanks than in the central magnetotail.

Substorm onset is generally assumed to initiate in some region of the magnetotail, whether at a near-Earth neutral line (Baker et al., 1996) or in the region between stretched and dipolar field lines with some current disruption (Lui, 1996). However, substorms are usually identified by their impact on the ionosphere through the enhancement of the westward electrojet as measured by ground magnetic deflections (Akasofu, 1968; Birkeland, 1908, 1913; Elvey, 1957), from auroral brightenings (Akasofu, 1964), or via the presence of ULF waves (Jacobs et al., 1964). These methods all allow the detection of the presence of a magnetospheric substorm at some unknown point after onset, whereupon information regarding the substorm has been communicated from the magnetosphere to the ionosphere. As such, there is an inherent uncertainty in time of the substorm in the magnetosphere compared to the time of onset in the ionosphere. This timing issue is then further exacerbated by measurement/technical uncertainties of the onset from auroral cameras and ground magnetometers. For example, Forsyth et al. (2015) showed that the SOPHIE technique provides substorm onsets that are predominantly within 20 min of auroral onsets. By taking this uncertainty into account, and assuming that the magnetic energy density immediately decreases at onset at any given location, we can explain the apparent plateaus in energy density seen close to substorm onset in our statistical averages that, at first glance, appear to be a stagnation of energy storage in the magnetotail at the cusp between the growth phase and the expansion phase.

Given that the plateau in the near-tail region occurs both before the zero epoch and before the plateaus at all radial distances then, even with ground onset uncertainty, this strongly suggests that the signatures of the substorm are first observed in the near-tail region before being observed in the ionosphere and elsewhere in the magnetotail. The plateau in magnetic energy density is seen in the mid-tail region at a time encompassing the onset time and, in the far-tail region, largely occurs following the ground onset. Our results strongly indicate that effects of substorm onset are first measured in the near-tail region, before being felt further downtail. Our results also highlight the particular difficulties in comparing space and ground-based measurements, as previous results have considered the lobes to be relatively homogeneous, whereas our results clearly show that information has to propagate away from the onset region, both down the magnetotail and toward the ground.

Each of the plotted superposed epoch analyses of ΔU_B shows a plateau that lasts $\sim$ 20 min. This plateau is immediately after substorm onset in Figure 1b and is before/centered on/after onset for the near-tail/mid-tail/far-tail data, respectively (Figure 3). Similar features have previously been seen in superposed epoch analyses of substorm onsets, which looked at the behavior of different physical quantities over the course of a substorm. A $\sim$ 20-min plateau was seen in a superposed epoch analysis of the average latitude of the Birkeland current ovals (Coxon et al., 2014a). This was attributed to the dayside and nightside reconnection rates being approximately equivalent after substorm onset, such that no expansion or contraction of the polar cap (for which the Birkeland current ovals are a proxy) occurred. We demonstrate in section 5 that this observation can be more simply explained by considering the uncertainty in time of a substorm onset identification. Assuming that the uncertainty on the substorm onset is $\pm$15 min, simulating 65 events with random lags within this range and then superposing them shows that this plateau can arise naturally simply from the uncertainty on the onset identification. This elegantly provides an alternative explanation for both our results and the results of Coxon et al. (2014a).

Previously, Caan et al. (1978) conducted a superposed epoch analysis of magnetic energy density in the magnetotail lobes using OGO-5 data and 240 substorm onsets (determined algorithmically). The uncertainty on their measurements is approximately equal to their observed change in magnetic energy density, so although their results are consistent with physical expectations, we cannot infer that they could not have come about by chance. Caan et al. (1978) first examined the superposed epoch analysis of all 240 events, finding that the energy density in the tail rose from 1 to 1.5 hr prior to expansion phase onset and showed that the energy density decayed for approximately 1–2 hr afterward. In our analysis of all 541 substorms (Figure 1b), we see ΔU_B increasing from $T = 75$ min until expansion phase onset, which is consistent with the increase in energy density seen from 1 to 1.5 hr prior to onset observed by Caan et al. (1978). However, in this superposition,

Caan et al. (1978) saw the energy density increase to onset and then decrease immediately after onset, which is not consistent with our observation of a 20-min-long plateau in the energy density.

Caan et al. (1978) also subdivided their analyses by distance of the spacecraft downtail, taking events that were within 25° of the $Y = 0R_E$ axis, and then subdivided into events in the range $-10 \geq X \geq -17R_E$ and events in the range $-17 \geq X \geq -20R_E$ to represent the near-tail (34 events) and far-tail (32). This makes it difficult to directly compare their results with ours, since C1 was located at $X > -17.4R_E$ for each of our substorm onsets. In contrast to our results, Caan et al. (1978) observe larger magnetic energy densities in their near-tail bin compared with their far-tail bin. We observe energy densities that are larger with distance downtail. Caan et al. (1978) do not detrend the data by removing the magnetic energy density due to spacecraft position. Since the magnetic field in the lobe is stronger closer to Earth, this means that the magnetic energy density will generally be stronger closer to Earth, so this may explain why their results disagree with ours in this regard. With respect to the lags we see between the three downtail distances, there is no obvious lag between Caan et al.'s (1978) near-tail and far-tail observations. This could be because they do not plot data closer to Earth than 10 R_E, they have a lower number of events in their bins (approximately half of ours), they have a relatively larger margin of error on their observations, or because of some combination of these effects.

Although we cannot measure the entire volume of the available energy in the magnetotail, using a simple cylinder of radius $15R_E$ and assuming an effective tail length of $50R_E$ (the same assumption used by Baker et al., 1997) gives a cylindrical volume of 9.14×10^{24} m^3. We emphasize that this is a crude estimate, as it does not take into account the flaring of the magnetotail, which flares until $\sim 100R_E$ (e.g., Slavin et al., 1985). Adding or removing magnetic flux from the magnetotail increases or decreases the flaring (Shukhtina et al., 2004), and we note that this effect is not considered in our calculations. Taking our decrease in substorm energy density, based on the results in Table 2, as at least 5×10^{-11} J/m^3, this gives a substorm energy of 4.57×10^{14}, which is approximately equal to the estimate given by Baker et al. (1997; 5×10^{14} J) but lower than that given by Østgaard et al. (2002; 7.7×10^{15} J). It is known that SOPHIE is able to detect expansion phase onsets for substorms with smaller signatures in ground magnetometer readings than in other onset lists (Forsyth et al., 2015), and this result indicates that the substorm analyzed by Baker et al. (1997) is closer in size to the substorms contributing to this analysis than the substorm of Østgaard et al. (2002), with respect to the amount of energy dissipated. Furthermore, this contradicts hypotheses claiming that the magnetotail is not an important source of energy for substorms (Akasofu, 2013, 2017) and supports criticism of those hypotheses (Miyashita et al., 2015), but it does not necessarily preclude the inner magnetosphere or plasma sheet (e.g., Forsyth et al., 2014) playing a key role.

7. Conclusions

We use magnetic field measurements from Cluster 1 to diagnose the energy density increase and decrease leading up to and following substorm onset during 541 isolated substorms. We fit a second-order polynomial to the observed magnetic energy density and removed it to isolate the substorm signature. The energy density increases until reaching a plateau for $\sim$ 20 min, which can be explained by modeling the uncertainty in substorm onset, and then decreases by at least 5×10^{-11} J/m^3 after substorm onset. Assuming that a simple cylinder accurately represents the volume of the magnetotail lobes, this gives an average dissipated energy of $\sim 5 \times 10^{14}$ J, which is consistent with the case study of Baker et al. (1997).

We subdivided the data spatially and generated three bins in which C1 was at increasing distances down the magnetotail at substorm onset. Plotting the superposed epoch analyses of these three subsets of the data and performing a cross-correlation analysis has allowed us to see that the mid-tail and far-tail bins lagged behind the near-tail bin by 19 and 21 min, respectively, indicating that the substorm signature of magnetic energy density starts near Earth and propagates down the magnetotail. The change in magnetic energy density also increases with distance downtail. This provides evidence for a phenomenological model of substorms in which some triggering mechanism occurs at a distance $X < 9R_E$ and then propagates both down the magnetotail and toward the ionosphere, and thus supports the CD model of substorms.

Acknowledgments
This work was supported by NERC joint grants NE/L007177/1 (J. C. C. and C. M. J.), NE/L006456/1 (M. P. F.), and NE/L007495/1 (C. F. and I. J. R.), in addition to STFC Ernest Rutherford grant ST/L002809/1 and Fellowship ST/K004298/2 (J. C. C. and R. C. F.) and NERC Independent Research FellowshipNE/N014480/1 (C. F.). Cluster data used in this paper were downloaded from the European Space Agency's Cluster and Double Star Science Archive (http://www.cosmos.esa.int/web/csa/access). SOPHIE data used in this paper were obtained from the supporting information of Forsyth et al. (2015). OMNI data used in this paper were obtained from CDAWeb (https://cdaweb.sci.gsfc.nasa.gov/). Data analysis and plotting were conducted in Python: The libraries used were NumPy and SciPy (van der Walt et al., 2011), Matplotlib (Hunter, 2007), Pandas (McKinney, 2010), and SpacePy (Morley et al., 2010).

References

Akasofu, S.-I. (1964). The development of the auroral substorm. *Planetary and Space Science*, *12*(4), 273–282. https://doi.org/10.1016/0032-0633(64)90151-5

Akasofu, S.-I. (1968). *Polar and magnetospheric substorms*. Dordrecht, Holland: D. Reidel Company. https://doi.org/10.1007/978-94-010-3461-6

Akasofu, S. I. (1981). Energy coupling between the solar wind and the magnetosphere. *Space Science Reviews*, *28*(2), 121–190. https://doi.org/10.1007/BF00218810

Akasofu, S.-I. (2013). Where is the magnetic energy for the expansion phase of auroral substorms accumulated? *Journal of Geophysical Research: Space Physics*, *118*, 7219–7225. https://doi.org/10.1002/2013JA019042

Akasofu, S.-I. (2017). *Where is the magnetic energy for the expansion phase of auroral substorms accumulated? II. The main body not the magnetotail* (Vol. 122, pp. 8479–8487). https://doi.org/10.1002/2016JA023074

Angelopoulos, V., McFadden, J. P., Larson, D., Carlson, C. W., Mende, S. B., Frey, H., et al. (2008). Tail reconnection triggering substorm onset. *Science*, *321*(5891), 931–935. https://doi.org/10.1126/science.1160495

Angelopoulos, V., McFadden, J. P., Larson, D., Carlson, C. W., Mende, S. B., Frey, H., et al. (2009). Response to comment on "Tail reconnection triggering substorm onset". *Science*, *324*(5933), 1391. https://doi.org/10.1126/science.1168045

Axford, W. (1999). Reconnection, substorms and solar flares. *Physics and Chemistry of the Earth, Part C: Solar, Terrestrial & Planetary Science*, *24*(1), 147–151. https://doi.org/10.1016/S1464-1917(98)00022-1

Baker, D. N., Fritz, T. A., McPherron, R. L., Fairfield, D. H., Kamide, Y., & Baumjohann, W. (1985). Magnetotail energy storage and release during the CDAW 6 substorm analysis intervals. *Journal of Geophysical Research*, *90*(A2), 1205–1216. https://doi.org/10.1029/JA090iA02p01205

Baker, D. N., Pulkkinen, T. I., Angelopoulos, V., Baumjohann, W., & McPherron, R. L. (1996). Neutral line model of substorms: Past results and present view. *Journal of Geophysical Research*, *101*(A6), 12,975–13,010. https://doi.org/10.1029/95JA03753

Baker, D. N., Pulkkinen, T. I., Hesse, M., & McPherron, R. L. (1997). A quantitative assessment of energy storage and release in the Earth's magnetotail. *Journal of Geophysical Research*, *102*(A4), 7159–7168. https://doi.org/10.1029/96JA03961

Birkeland, K. (1908). *The Norwegian Aurora Polaris Expedition 1902–1903*. (Vol. 1) Christiania, Norway: H. Aschelhoug & Co.

Birkeland, K. (1913). *The Norwegian Aurora Polaris Expedition 1902–1903*. (Vol. 2) Christiania, Norway: H. Aschelhoug & Co.

Browett, S. D., Fear, R. C., Grocott, A., & Milan, S. E. (2017). Timescales for the penetration of IMF B_y into the Earth's magnetotail. *Journal of Geophysical Research: Space Physics*, *122*, 579–593. https://doi.org/10.1002/2016JA023198

Caan, M. N., McPherron, R. L., & Russell, C. T. (1973). Solar wind and substorm-related changes in the lobes of the geomagnetic tail. *Journal of Geophysical Research*, *78*(34), 8087–8096. https://doi.org/10.1029/JA078i034p08087

Caan, M. N., McPherron, R. L., & Russell, C. T. (1975). Substorm and interplanetary magnetic field effects on the geomagnetic tail lobes. *Journal of Geophysical Research*, *80*(1), 191–194. https://doi.org/10.1029/JA080i001p00191

Caan, M. N., McPherron, R. L., & Russell, C. T. (1978). The statistical magnetic signature of magnetospheric substorms. *Planetary and Space Science*, *26*(3), 269–279. https://doi.org/10.1016/0032-0633(78) 90092-2

Clausen, L. B. N., Baker, J. B. H., Ruohoniemi, J. M., Milan, S. E., & Anderson, B. J. (2012). Dynamics of the region 1 Birkeland current oval derived from the Active Magnetosphere and Planetary Electrodynamics Response Experiment (AMPERE). *Journal of Geophysical Research*, *117*, A06233. https://doi.org/10.1029/2012JA017666

Cowley, S. W. H., & Lockwood, M. (1992). Excitation and decay of solar wind-driven flows in the magnetosphere-ionosphere system. *Annales Geophysicae*, *10*, 103–115.

Coxon, J. C., Jackman, C. M., Freeman, M. P., Forsyth, C., & Rae, I. J. (2016). Identifying the magnetotail lobes with Cluster magnetometer data. *Journal of Geophysical Research: Space Physics*, *121*, 1436–1446. https://doi.org/10.1002/2015JA022020

Coxon, J. C., Milan, S. E., Carter, J. A., Clausen, L. B. N., Anderson, B. J., & Korth, H. (2016). Seasonal and diurnal variations in AMPERE observations of the Birkeland currents compared to modeled results. *Journal of Geophysical Research: Space Physics*, *121*, 4027–4040. https://doi.org/10.1002/2015JA022050

Coxon, J. C., Milan, S. E., Clausen, L. B. N., Anderson, B. J., & Korth, H. (2014a). A superposed epoch analysis of the regions 1 and 2 Birkeland currents observed by AMPERE during substorms. *Journal of Geophysical Research: Space Physics*, *119*, 9834–9846. https://doi.org/10.1002/2014JA020500

Coxon, J. C., Milan, S. E., Clausen, L. B. N., Anderson, B. J., & Korth, H. (2014b). The magnitudes of the regions 1 and 2 Birkeland currents observed by AMPERE and their role in solar wind-magnetosphere-ionosphere coupling. *Journal of Geophysical Research: Space Physics*, *119*, 9804–9815. https://doi.org/10.1002/2014JA020138

DeJong, A. D., Cai, X., Clauer, R. C., & Spann, J. F. (2007). Aurora and open magnetic flux during isolated substorms, sawteeth, and SMC events. *Annales Geophysicae*, *25*(8), 1865–1876. https://doi.org/10.5194/angeo-25-1865-2007

Dungey, J. W. (1961). Interplanetary magnetic field and the auroral zones. *Physics Review Letters*, *6*, 47–48.

Elvey, C. T. (1957). Problems in auroral morphology. *Proceedings of the National Academy of Sciences of the United States of America*, *43*(1), 63–75.

Escoubet, C. P., Fehringer, M., & Goldstein, M. (2001). The Cluster mission. *Annales Geophysicae*, *19*(10/12), 1197–1200. https://doi.org/10.5194/angeo-19-1197-2001

Forsyth, C., Rae, I. J., Coxon, J. C., Freeman, M. P., Jackman, C. M., Gjerloev, J., & Fazakerley, A. N. (2015). A new technique for determining Substorm Onsets and Phases from Indices of the Electrojet (SOPHIE). *Journal of Geophysical Research: Space Physics*, *120*, 10,592–10,606. https://doi.org/10.1002/2015JA021343

Forsyth, C., Rae, I. J., Murphy, K. R., Freeman, M. P., Huang, C.-L., Spence, H. E., et al. (2016). What effect do substorms have on the content of the radiation belts? *Journal of Geophysical Research: Space Physics*, *121*, 6292–6306. https://doi.org/10.1002/2016JA022620

Forsyth, C., Watt, C. E. J., Rae, I. J., Fazakerley, A. N., Kalmoni, N. M. E., Freeman, M. P., et al. (2014). Increases in plasma sheet temperature with solar wind driving during substorm growth phases. *Geophysical Research Letters*, *41*, 8713–8721. https://doi.org/10.1002/2014GL062400

Freeman, M. P., & Morley, S. K. (2009). No evidence for externally triggered substorms based on superposed epoch analysis of IMF B_z. *Geophysical Research Letters*, *36*, L21101. https://doi.org/10.1029/2009GL040621

Freeman, M., & Southwood, D. (1988). The effect of magnetospheric erosion on mid- and high-latitude ionospheric flows. *Planetary and Space Science*, *36*(5), 509–522. https://doi.org/10.1016/0032-0633(88)90110-9

Holzer, R. E., McPherron, R. L., & Hardy, D. A. (1986). A quantitative empirical model of the magnetospheric flux transfer process. *Journal of Geophysical Research*, *91*(A3), 3287–3293. https://doi.org/10.1029/JA091iA03p03287

Holzer, R. E., & Slavin, J. A. (1979). A correlative study of magnetic flux transfer in the magnetosphere. *Journal of Geophysical Research*, *84*(A6), 2573–2578. https://doi.org/10.1029/JA084iA06p02573

Hones, E. W. (1979). Transient phenomena in the magnetotail and their relation to substorms. *Space Science Reviews*, *23*(3), 393–410. https://doi.org/10.1007/BF00172247

Hsieh, M.-S., & Otto, A. (2014). The influence of magnetic flux depletion on the magnetotail and auroral morphology during the substorm growth phase. *Journal of Geophysical Research: Space Physics*, *119*, 3430–3443. https://doi.org/10.1002/2013JA019459

Hsieh, M.-S., & Otto, A. (2015). Thin current sheet formation in response to the loading and the depletion of magnetic flux during the substorm growth phase. *Journal of Geophysical Research: Space Physics*, *120*, 4264–4278. https://doi.org/10.1002/2014JA020925

Hubert, B., Milan, S. E., Grocott, A., Blockx, C., Cowley, S. W. H., & Gérard, J.-C. (2006). Dayside and nightside reconnection rates inferred from IMAGE FUV and Super Dual Auroral Radar Network data. *Journal of Geophysical Research*, *111*, A03217. https://doi.org/10.1029/2005JA011140

Hunter, J. D. (2007). Matplotlib: A 2D graphics environment. *Computing in Science & Engineering*, *9*(3), 90–95. https://doi.org/10.1109/MCSE.2007.55

Ieda, A., Machida, S., Mukai, T., Saito, Y., Yamamoto, T., Nishida, A., et al. (1998). Statistical analysis of the plasmoid evolution with Geotail observations. *Journal of Geophysical Research*, *103*(A3), 4453–4465. https://doi.org/10.1029/97JA03240

Jacobs, J. A., Kato, Y., Matsushita, S., & Troitskaya, V. A. (1964). Classification of geomagnetic micropulsations. *Journal of Geophysical Research*, *69*(1), 180–181. https://doi.org/10.1029/JZ069i001p00180

Kallio, E. I., Pulkkinen, T. I., Koskinen, H. E. J., Viljanen, A., Slavin, J. A., & Ogilvie, K. (2000). Loading-unloading processes in the nightside ionosphere. *Geophysical Research Letters*, *27*(11), 1627–1630. https://doi.org/10.1029/1999GL003694

Kalmoni, N. M. E., Rae, I. J., Murphy, K. R., Forsyth, C., Watt, C. E. J., & Owen, C. J. (2017). Statistical azimuthal structuring of the substorm onset arc: Implications for the onset mechanism. *Geophysical Research Letters*, *44*, 2078–2087. https://doi.org/10.1002/2016GL071826

Lockwood, M., & Cowley, S. W. H. (1992). Ionospheric convection and the substorm cycle, *Substorms 1: Proceedings of the First International Conference on Substorms* (Vol. 1, pp. 99–109). Kiruna, Sweden: European Space Agency.

Lui, A. T. Y. (1996). Current disruption in the Earth's magnetosphere: Observations and models. *Journal of Geophysical Research*, *101*(A6), 13,067–13,088. https://doi.org/10.1029/96JA00079

Lui, A. T. Y. (2009). Comment on "Tail reconnection triggering substorm onset". *Science*, *324*(5933), 1391–1391. https://doi.org/10.1126/science.1167726

Lui, A. T. Y., Lopez, R. E., Anderson, B. J., Takahashi, K., Zanetti, L. J., McEntire, R. W., et al. (1992). Current disruptions in the near-Earth neutral sheet region. *Journal of Geophysical Research*, *97*(A2), 1461–1480. https://doi.org/10.1029/91JA02401

McKinney, W. (2010). Data structures for statistical computing in Python. In S. van der Walt & J. Millman (Eds.), *Proceedings of the 9th Python in Science Conference (SciPy 2010)* (pp. 51–56). Austin, TX.

McPherron, R. L. (1970). Growth phase of magnetospheric substorms. *Journal of Geophysical Research*, *75*(28), 5592–5599. https://doi.org/10.1029/JA075i028p05592

McPherron, R. L., Russell, C. T., & Aubry, M. P. (1973). Satellite studies of magnetospheric substorms on August 15, 1968: 9. Phenomenological model for substorms. *Journal of Geophysical Research*, *78*(16), 3131–3149. https://doi.org/10.1029/JA078i016p03131

Milan, S. E., Gosling, J. S., & Hubert, B. (2012). Relationship between interplanetary parameters and the magnetopause reconnection rate quantified from observations of the expanding polar cap. *Journal of Geophysical Research*, *117*, A03226. https://doi.org/10.1029/2011JA017082

Milan, S. E., Grocott, A., Forsyth, C., Imber, S. M., Boakes, P. D., & Hubert, B. (2009). A superposed epoch analysis of auroral evolution during substorm growth, onset and recovery: Open magnetic flux control of substorm intensity. *Annales Geophysicae*, *27*(2), 659–668. https://doi.org/10.5194/angeo-27-659-2009

Milan, S. E., Provan, G., & Hubert, B. (2007). Magnetic flux transport in the Dungey cycle: A survey of dayside and nightside reconnection rates. *Journal of Geophysical Research*, *112*, A01209. https://doi.org/10.1029/2006JA011642

Miyashita, Y., Machida, S., Kamide, Y., & Nishida, A. (2015). Comment on "Where is the magnetic energy for the expansion phase of auroral substorms accumulated?" by S.-I. Akasofu. *Journal of Geophysical Research: Space Physics*, *120*, 3827–3828. https://doi.org/10.1002/2014JA020841

Morley, S. K., Koller, J., Welling, D. T., Larsen, B. A., Henderson, M. G., & Niehof, J. T. (2010). SpacePy—A Python-based library of tools for the space sciences. In S. van der Walt, J. Millman (Eds.), *Proceedings of the 9th Python in Science Conference (SciPy 2010)* (pp. 39–45). Austin, TX.

Newell, P. T., & Gjerloev, J. W. (2011). Evaluation of SuperMAG auroral electrojet indices as indicators of substorms and auroral power. *Journal of Geophysical Research*, *116*, A12211. https://doi.org/10.1029/2011JA016779

Nishimura, Y., Yang, J., Pritchett, P. L., Coroniti, F. V., Donovan, E. F., Lyons, L. R., et al. (2016). Statistical properties of substorm auroral onset beads/rays. *Journal of Geophysical Research: Space Physics*, *121*, 8661–8676. https://doi.org/10.1002/2016JA022801

Østgaard, N., Germany, G., Stadsnes, J., & Vondrak, R. R. (2002). Energy analysis of substorms based on remote sensing techniques, solar wind measurements, and geomagnetic indices. *Journal of Geophysical Research*, *107*(A9), 1233. https://doi.org/10.1029/2001JA002002

Perreault, P., & Akasofu, S. I. (1978). A study of geomagnetic storms. *Geophysical Journal International*, *54*(3), 547–573. https://doi.org/10.1111/j.1365-246X.1978.tb05494.x

Shukhtina, M. A., Dmitrieva, N. P., & Sergeev, V. A. (2004). Quantitative magnetotail characteristics of different magnetospheric states. *Annales Geophysicae*, *22*(3), 1019–1032. https://doi.org/10.5194/angeo-22-1019-2004

Siscoe, G. L., & Huang, T. S. (1985). Polar cap inflation and deflation. *Journal of Geophysical Research*, *90*(A1), 543–547. https://doi.org/10.1029/JA090iA01p00543

Slavin, J. A., Smith, E. J., Sibeck, D. G., Baker, D. N., Zwickl, R. D., & Akasofu, S.-I. (1985). An ISEE 3 study of average and substorm conditions in the distant magnetotail. *Journal of Geophysical Research*, *90*(A11), 10,875–10,895. https://doi.org/10.1029/JA090iA11p10875

Snekvik, K., Tanskanen, E., Østgaard, N., Juusola, L., Laundal, K., Gordeev, E. I., & Borg, A. L. (2012). Changes in the magnetotail configuration before near-Earth reconnection. *Journal of Geophysical Research*, *117*, A02219. https://doi.org/10.1029/2011JA017040

Sun, W. J., Fu, S. Y., Wei, Y., Yao, Z. H., Rong, Z. J., Zhou, X. Z., et al. (2017). Plasma sheet pressure variations in the near-Earth magnetotail during substorm growth phase: THEMIS observations. *Journal of Geophysical Research: Space Physics*, *122*, 12,212–12,228. https://doi.org/10.1002/2017JA024603

Tanskanen, E., Pulkkinen, T. I., Koskinen, H. E. J., & Slavin, J. A. (2002). Substorm energy budget during low and high solar activity: 1997 and 1999 compared. *Journal of Geophysical Research*, *107*(A6), 1086. https://doi.org/10.1029/2001JA900153

van der Walt, S., Colbert, S. C., & Varoquaux, G. (2011). The NumPy array: A structure for efficient numerical computation. *Computing in Science & Engineering*, *13*(2), 22–30. https://doi.org/10.1109/MCSE.2011.37

Walker, R. J., & Russell, C. T. (1995). Solar-wind interactions with magnetized planets. In M. G. Kivelson & C. T. Russell (Eds.), *Introduction to space physics* (Chap. 6, pp. 164–182). Cambridge, UK: Cambridge University Press.

Weiss, L. A., Reiff, P. H., Moses, J. J., Heelis, R. A., & Moore, B. D. (1992). *Energy dissipation in substorms*.

Erratum

Errors introduced during typesetting have been corrected in this version. In particular, instances of "SML" have been italicized. In the fifth paragraph of the Introduction, "«SPI-I20»" has been corrected as E_{002}. In the sixth paragraph of the Introduction, "«SPI-I63»" has been corrected to $<10R_E$. The present version may be considered the authoritative version of record.